China Instrument and Control Society
Instrumentation
OPEN ACCESS
INSTRUMENTATION, Vol. 12, No. 2, June 2025 https://doi.org/10.15878/j.instr.202500287

Article

Study on the Correction Method of Radiant Temperature Measurement of Turbine Blades Under the Background of High-Temperature Dynamics

Shengnan Liu*, Liwei Chen

College of Information and Communication Engineering, Harbin Engineering University, Harbin 150001, China

* Corresponding author email: asd25802025@163.com

Abstract: The turbine blades operate under high temperature and high pressure conditions, and when using radiation thermometry, the influence of radiation from surrounding blades leads to measurement errors. To address this issue, this paper develops a three-dimensional discretized dynamic radiation transfer model based on the blade shape of the turbine. The relationship between the radiation angle coefficient of the surrounding blades and the rotation angle of the blade under test is analyzed. The radiation angle coefficient is calculated using the triangular element method, and temperature inversion is performed based on the effective emissivity to compute the measurement error. The results show that under dynamic high temperature conditions, the temperature measurement error caused by reflection at the selected 60% leaf height point varies with the rotation angle , and the maximum reaches 25.58K. The angular coefficient exhibits periodic fluctuations with changes in rotation angle, and the maximum effective emissivity increases as the rotation angle increases. As the blade height increases, the impact of reflected radiation on radiometric temperature measurement errors shows a decreasing trend.This study provides a reference for radiation thermometry in dynamic high-temperature environments.

Keywords: radiation temperature measurement; dynamic background; turbine blades; effective emissivity; error

Citation: Shengnan Liu, Liwei Chen."Study on the Correction Method of Radiant Temperature Measurement of Turbine Blades Under the Background of High-Temperature Dynamics." Instrumentation 12, no.2 (June 2025). https://doi.org/10.15878/j.instr.202500287

1 Introduction

The aircraft engine and gas turbine are highly complex and precise thermo-mechanical systems that convert chemical energy into mechanical energy[1-3], serving as the primary source of power[4,5]. As a critical component of the engine[6,7], turbine blades operate under extreme conditions of high temperature and high pressure for extended periods[8,9]. However, excessively high temperatures can lead to engine failures[10]. To ensure the normal operation of the engine, accurately measuring the surface temperature of the turbine blades is of great significance[11-13]. Currently, radiation thermometry technology, with its advantages of non-contact measurement and fast response[14,15], is widely used for measuring the temperature of turbine blades[16].

In high-temperature environments, when using radiation thermometry to measure the temperature of turbine blades, the obtained thermal radiation signals not only originate from the radiation characteristics of the measured blade itself but are also influenced by the reflected radiation from the surrounding environment. This reflected radiation can introduce significant measurement errors. Therefore, when performing temperature measurements, it is essential to fully consider the interference of these background reflections on the

signal to improve the accuracy and reliability of the measurements[17]. Many scholars have conducted related research on this issue. De Lucia established a simplified turbine blade model for simulated temperature measurements, dividing the surface of the object into rectangular elements and introducing the angle coefficient to calculate the reflected radiation in a high-temperature environment[18]. However, this study was based on a simplified two-dimensional turbine blade model, and the research was limited to the impact of reflected radiation under static conditions. The team led by Fu Tairan studied the variation patterns of reflected radiation in turbine blade radiation thermometry and analyzed the effective emissivity distribution of turbine blades under different wavelength and emissivity conditions[19]. However, these studies focused on temperature error measurements under static conditions and did not address the impact of background radiation on measurement errors during dynamic operation. Gao et al. simulated the background blade temperature distribution using ANSYS(Analysis System) and calculated the angle coefficients between blade surface elements using formula-based methods. They proposed the variation pattern of high-temperature background radiation in turbine blade operation[20,21]. However, when calculating the reflected radiation from the surrounding blades to the blade under test, they assumed the blades had an isothermal distribution, whereas the actual temperature distribution of the blades is non-isothermal. Zheng et al**.** considered the geometric shape and operational state of the blades and, through solving the angle coefficients between the environment and the blade surface and performing discrete coordinate transformations, developed a three-dimensional dynamic reflection radiation analysis model for turbine blades. This method effectively eliminates the influence of reflected radiation[22]. However, this approach discretizes the blade surface using small rectangular elements, which cannot accurately describe the complex shape of the blades, and the calculation efficiency of the angle coefficients is relatively low.

For the deficiencies in the above studies, the main innovations and contributions of this paper are as follows: (1) Based on the cyclic motion characteristics of the blade, a dynamic three-dimensional model of the rotation angle dependence is constructed, which reveals the law that the angular coefficient changes with the angle. The proposed model overcomes the defect that the static model cannot reflect the dynamic change of reflected radiation during rotation. Meanwhile, the scope of application is wider. (2) The traditional rectangular surface element method has poor geometric fitness and does not consider the dynamic masking effect. In this paper, the proposed triangular surface element discretization can more accurately characterize the surface structure and temperature distribution of the turbine blade, and combined with the visual masking judgment for the screening of surface elements, so that the computational efficiency can be improved. (3) The concept of effective emissivity is introduced to quantitatively analyze the influence of the surrounding reflected radiation on the temperature measurement error of the moving blade to be measured under different rotation angles. The radiation measured by pyrometer can be used to directly solve the target temperature to be measured, thus realizing fast temperature calculation.

Specifically, based on the relative position and layout characteristics of the turbine blades, a typical blade is selected for analysis, and a model matching it is established to simulate the operation process of the turbine blade. Considering the periodic spatial arrangement distribution characteristics and motion characteristics of the turbine blades, this study only analyzes the operation process of the moving blade to be measured in one complete cycle, focusing on the influence of the surrounding high temperature background on the suction surface of the moving blade to be measured. The triangular surface element method is used to calculate the angular coefficients to accurately characterize the structural features and temperature distribution of the component surfaces. The discrete face elements are judged by masking so as to filter out the face elements that need to be calculated in order to improve the computational efficiency. Meanwhile, the effective emissivity is introduced and the distribution of the effective emissivity at different rotation angles under the dynamic background is determined by calculation. The study further analyzes the influence of the surrounding reflected radiation on the temperature measurement error of the dynamic lobe to be measured at different rotation angles.

2 Materials and Methods

2.1 Basic Theory

Planck's blackbody radiation law states that the blackbody radiation energy is wavelength and temperature dependent, and the expression can be expressed by Equation (1):

$$M(\lambda, T) = c_1 \lambda^{-5} (e^{c_2/\lambda T} - 1)^{-1} \tag{1}$$

Where $c_1 = 3.7418 \times 10^{-16}\,\mathrm{W \cdot m^2}$ is the first Planck constant, $c_2 = 1.4388 \times 10^{-2}\,\mathrm{m \cdot K}$ is the second Planck constant, λ is the measured wavelength. Monochromatic thermometry is one of the methods of radiometric thermometry, also known as brightness thermometry, which is the measurement of the radiant energy of the object to be measured in a specific wavelength range.The brightness temperature T is calculated as shown in Equation (2):

$$c_1 \lambda^{-5} (e^{c_2/\lambda T} - 1)^{-1} = \varepsilon_\lambda c_1 \lambda^{-5} (e^{c_2/\lambda T_b} - 1)^{-1} \tag{2}$$

Where T is the temperature obtained by using monochromatic thermometry, T_b is the true temperature of

the object to be measured, $\varepsilon_\lambda$is the emissivity at the wavelength λ condition. The relationship between the bright temperature T measured by monochromatic thermometry and the true temperature T_b have the following relationship:

$$\frac{1}{T}-\frac{1}{T_b}=\frac{\lambda}{C_2}\ln\left(\frac{1}{\varepsilon_\lambda}\right) \tag{3}$$

Therefore if the value of the target emissivity is known, the solution of the true temperature can be realized. However, when the temperature of the target blade to be measured is measured by radiometric thermometry in a high temperature background, the radiant energy obtained from brightness thermometry is shown in Equation (4) due to the effect of reflected radiation from the high temperature background:

$$M(\lambda,T)=\varepsilon_\lambda M(\lambda,T_b)+(1-\varepsilon_\lambda)M(\lambda,T_r) \tag{4}$$

Where $M(\lambda,T)$ is the total amount of radiation received by the detector. Where $M(\lambda,T_b)$ is the blackbody radiation emissivity of the target to be measured. Where $M(\lambda,T_r)$ is the radiant emissivity of the high temperature environment to the surface of the target to be measured. The value of $(1-\varepsilon_\lambda)$ is equal to the reflectance of the surface of the turbine blade of non-transparent material, so the effect of background reflection needs to be taken into account.

2.2 Turbine Blade Reflection Analysis Transmission Model

Due to the presence of high-temperature components such as the front-stage guide vanes and adjacent moving blades, the radiation signals received by the infrared detector include not only the radiation from the target blade under test but also interference from the reflected radiation of the surrounding hot-end components. This leads to significant temperature measurement errors. Therefore, eliminating the influence of background reflection is crucial for improving measurement accuracy. In order to quantitatively analyze the reflection interference of the high temperature background (e.g., the front guide vane and the adjacent moving blade) from the radiation temperature measurement of the turbine blade to be measured during the rotating process of the moving blade. This study analyzes the turbine blade based on the UG (Unigraphics NX) model of the turbine disk, and the mesh delineation of the surface of the turbine blade is performed by adopting the method of triangular faceted element discretization, and the coordinate information of the triangular faceted element as well as the normal vector is subsequently are stored in the form of STL files. Fig. 1 shows a turbine disc consisting of 86 moving blades. During the rotation of the turbine blades, the moving blades undergo a circular motion around the x-axis in the yoz plane, with an angular difference of approximately 4.2° between adjacent moving blades. Since the blade structures are similar and the high-temperature environment of blades at the same stage is comparable, when a moving blade rotates by approximately 4.2°, it reaches the position of an adjacent moving blade. This can be considered as a cycle for analysis. In this study, two adjacent moving blades and the front-stage guide vanes are selected as research objects. The model of reflected radiation is based on the relative positional relationship between the blades, as shown in Fig. 2. Fig. 3 shows the cross-sectional view of the moving blade and guide vane obtained at 50% of the blade height. Fig. 4 illustrates the discretization of a typical blade. Due to the irregular shape of the turbine blades and the non-isothermal working environment, this study discretizes the blade surface using triangular elements, transforming the complex non-isothermal surface into a micro-surface with isothermal structure.

Fig.1 Complete turbine disk distribution

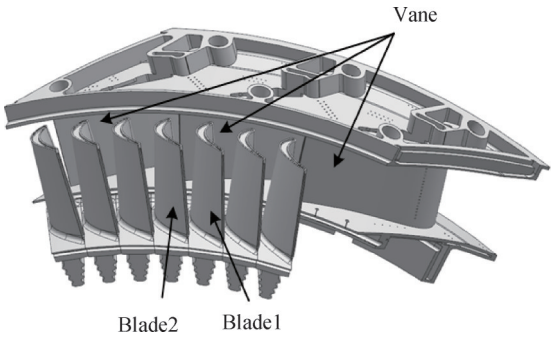

Fig.2 Partial turbine disk model

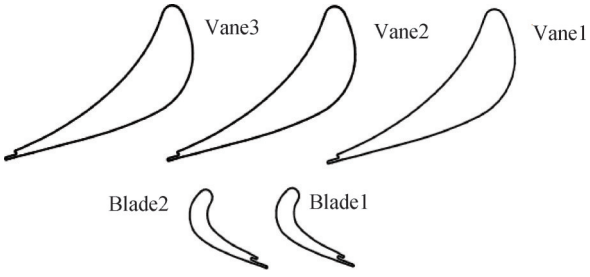

Fig.3 Cross-section of moving and static blades at 50% leaf height

To study the impact of dynamic background reflection during the rotation process on radiation thermometry, it is necessary to simulate the actual

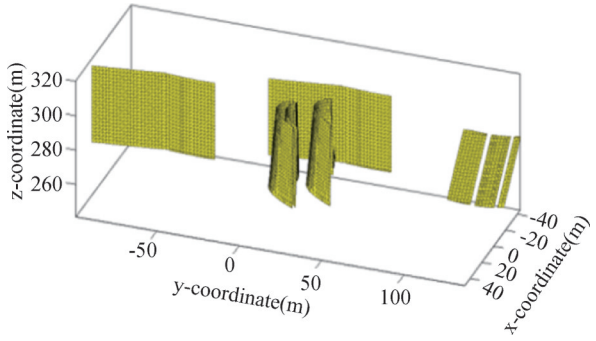

Fig.4 Typical blade discretization

relative positions of the turbine blades during dynamic rotation, as shown in Fig. 5. Since the guide vanes and moving blades are periodically distributed, this study analyzes the movement of the moving blade within one cycle. A geometric model is constructed based on the suction surface of the target moving blade, the adjacent moving blade above it, and the three preceding guide blades. In Fig. 5, the movement direction of the target moving blade is set to be opposite to the positive y-axis direction. The initial position of the simulated movement is set at the lowest point of the suction surface y-value of the target moving blade and aligned with the trailing edge of guide blade 1. At this point, the rotation angle is set to 0°. The target moving blade then rotates in the specified direction until it reaches the position of the adjacent moving blade, corresponding to a rotation angle of approximately 4.2° , which marks the end of the simulation. During dynamic operation, the variation in radiation from the guide blades received by the target blade is depicted in Fig. 5(a) – (c). In the simulation results, the positive direction of the x-axis points from the leading edge to the trailing edge of the moving blade, while the positive direction of the y-axis is opposite to the simulation movement direction. The measurement point P_0, located on the suction surface of the moving blade, is chosen as the reference point. As the target blade rotates, the radiation from the surrounding blades at the specific

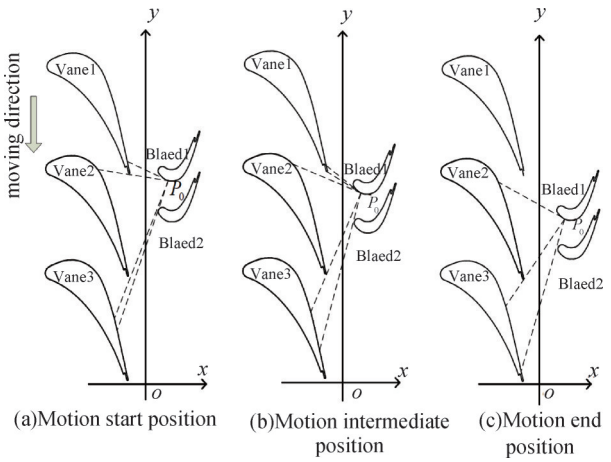

Fig.5 Schematic diagram of the change of motion in one cycle (a) Motion start position(b) Motion intermediate position(c) Motion end position

point P_0 changes. Different areas in Fig. 5 represent the influence of various surrounding blades on the radiation at the measured P_0 point.

In one motion cycle, the movement variation of the moving blade can be studied, and the transformation relationship of the surface coordinates at different positions when the moving blade rotates can be analyzed to describe the surface of the moving blade at different locations. The schematic diagram of the moving blade rotating counterclockwise around the x-axis is shown in Fig. 6.

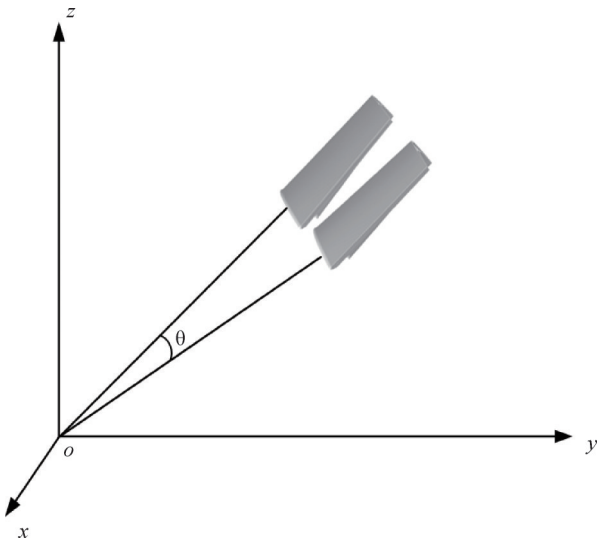

Fig.6 Relative position of moving blades at different positions

If a point has coordinates(x, y, z)in three-dimensional space, then the new coordinates(x', y', z')after rotating by an angle around the x-axis can be calculated using the following rotation matrix, as shown in Equation (5):

$$\begin{pmatrix} x' \\ y' \\ z' \end{pmatrix} = \begin{pmatrix} 1 & 0 & 0 \\ 0 & \cos(\theta) & -\sin(\theta) \\ 0 & \sin(\theta) & \cos(\theta) \end{pmatrix} \begin{pmatrix} x \\ y \\ z \end{pmatrix} \tag{5}$$

Therefore, after obtaining the position information of the turbine blade surface, the coordinate information during the rotation process of the moving blade can be derived from Equation (5), thereby establishing the three-dimensional dynamic reflection transfer model. To study the reflected radiation effects of the preceding guide vanes and adjacent moving blades on the target moving blade, it is necessary to calculate the radiation viewfactor between the discretized surface elements of the target moving blade and the adjacent blade surface elements, thus quantitatively describing the radiation influence of the surrounding blades on the target moving blade.

2.3 Calculation of viewfactor

In the case of high-temperature backgrounds, especially when the background temperature is higher than the target temperature, the influence of the background reflection on the measurement results must be considered. In order to minimize the interference

caused by background reflections, it is necessary to calculate the reflected energy produced by the background on the target surface. The calculation of the radiance viewfactors between individual discrete surface elements and the radiance of the surface elements themselves is the key step, which is the basis for solving for the reflected radiance of the environment at the point to be measured. The radiation viewfactor$F_{ji}$is the percentage of the radiant energy directly projected from the face element*j*onto the face element *i*to the total energy radiated by the face element*j*itself. The radiation viewfactor between the face elements is only related to the relative spatial position between the face elements and is independent of the parameters such as the temperature and the measured wavelength. In this paper, the viewfactors are calculated using the triangular face element method,while the values of the angular system at different angles are calculated by combining the equations of motion of the discrete face elements.

The simplified model in Fig. 4 is chosen as the study object and its viewfactors are calculated as shown in Fig. 7. Triangles are used as basic surface elements to discretize the blade surface. Each small triangle is assumed to have a uniform distribution of its temperature and radiant heat physical property parameters. Considering the workload and running speed of the calculation program, 2mm² triangular face elements are selected for discretization, which can accurately reflect the geometric structure and temperature distribution characteristics of the blade and effectively reduce the calculation time, and the viewfactor between the face elements can be solved according to the definition of the viewfactors of the triangular face elements.

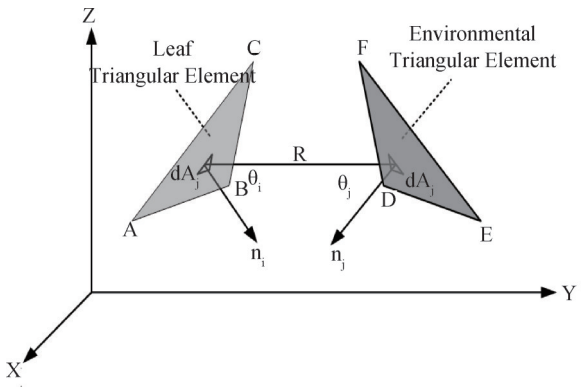

Fig.7 Calculation of viewfactors by microelements

Where A_i and A_j are the two triangular face elements of the turbine blade, dA_i and dA_j are the internal face micromeres of the two face elements, $\vec{n_i}$ and $\vec{n_j}$ are the normal vectors of the two face elements, θ_i and θ_j are the angles between the lines connecting the face micromeres and the corresponding normal vectors, and R is the center distance between the two face micromeres. Therefore the radiation viewfactor F_{ji} from the triangular face element A_j to the face element A_i of the turbine blade is calculated as in Equation (6).

$$F_{ji}=\frac{1}{A_j}\int_{A_i}\int_{A_j}\frac{\cos\theta_i\cos\theta_j dA_i dA_j}{\pi S^2} \tag{6}$$

Before calculating the viewfactor, to improve computational efficiency, it is necessary to filter the surface elements. First, a visual judgment is made to determine whether the two surfaces are mutually visible. If the two surfaces are visible, it is then necessary to verify whether the normal vectors of the surfaces and the vector formed by connecting the centers of the two surfaces satisfy Equation (7).

$$(\vec{n_i}\cdot\vec{R}>0)\&\&(-\vec{n_j}\cdot\vec{R}>0) \tag{7}$$

If the two surfaces are not visible to each other, the normal vector of each surface and the vector representing the line connecting their centers satisfy Equation (8).

$$(\vec{n_i}\cdot\vec{R}\le 0)\|(-\vec{n_j}\cdot\vec{R}\le 0) \tag{8}$$

In the equation, $\vec{n_i}$ and $\vec{n_j}$ are the normal vectors pointing outward from the environmental surface element and the surface element under test, respectively, and R is the vector connecting the centers of the two surface elements. After the initial screening, the occlusion effect of intermediate objects must also be considered, and the calculation results need to be corrected. The judgment steps are as follows: First, check whether the line connecting the centroids of the two triangles intersects with the plane of the third triangle. If they intersect, calculate the intersection point and check whether the intersection point lies inside the triangle. If an intermediate object occludes the line, the angle coefficient between the two surfaces is set to 0.

2.4 Reflected Radiometric Thermometry Corrections

The reflected radiation generated by the high-temperature background can severely affect the calculation of effective emissivity and temperature measurements during the radiation thermometry process. Therefore, it is necessary to calculate the reflected radiation of the target moving blade at different rotational positions. After calculating the radiation viewfactor of the surrounding environment blades using Equation (6), the theoretical temperature distribution of the preceding moving blades and guide vanes is set. The temperature field of the preceding moving blade is 833.15K, and the simulated temperature distribution of the preceding guide vanes is shown in Fig. 8[23].

After the reflection model is established, Equation (9) is used

$$M_i(\lambda,T_r)=\frac{1}{A_i}\sum_{j=1}^{N}A_j F_{ji} M_j(\lambda,T_j) \tag{9}$$

Where N is the number of turbine blade environmental surface elements, $M_j(\lambda,T_j)$ is the radiative outflow of each environmental surface element, T_j is the theoretical temperature value for high temperature environments A_i and A_j are the areas of the corresponding face elements.

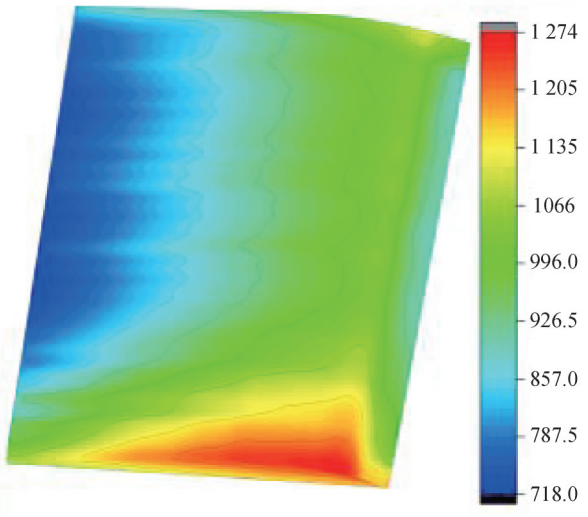

Fig.8 Theoretical temperature distribution field of the front stage guide vane

After calculating the amount of radiation from the high-temperature background ambient radiation, the emissivity of the surface of the surface element to be measured is set, and the amount of reflected radiation formed by the high-temperature ambient radiation on the surface of the blade to be measured is calculated according to Equation (10).

$$M_{r,i}(\lambda, T_r)=(1-\varepsilon_\lambda)\left(\sum_{j=1}^{N}\frac{A_j}{A_i}F_{ji}M_j(\lambda, T_j)\right) \tag{10}$$

Equation (11) calculates the amount of reflected radiation received by the pyrometer.

$$M(\lambda, T)=\varepsilon_\lambda M(\lambda, T_b)+M_{r,i}(\lambda, T_r) \tag{11}$$

By using the previously obtained values of the viewfactors of the moving blade to be measured at different angles during one cycle of rotation, it is therefore possible to calculate the reflected energy from the surroundings on the surface of the target blade at different angles of rotation.

From the above, it is known that in the high temperature state around the hot end components will have a great impact on the temperature measurement, in order to realize the correction of the reflection radiation temperature measurement error, further introduction of the concept of effective emissivity, the calculation method is shown in Equations (12) and (13):

$$M(\lambda, T)=\varepsilon_\lambda M(\lambda, T_b)+(1-\varepsilon_\lambda)M(\lambda, T_r)=\varepsilon_{eff}\cdot M(\lambda, T_b) \tag{12}$$

$$\varepsilon_{eff}=\frac{M(\lambda, T)}{M(\lambda, T_b)}=\frac{\varepsilon_\lambda\cdot M(\lambda, T_b)+(1-\varepsilon_\lambda)M(\lambda, T_r)}{M(\lambda, T_b)} \tag{13}$$

Where ε_{eff} refers to the effective emissivity of the turbine blade surface at wavelength λ. From Equations (10) and (13), the effective emissivity ε_{eff} is related to the actual emissivity $\varepsilon$of the blade surface and the angular coefficient between the surface $F_{j\,i}$ and the temperature. And by using Planck's formula, the $M(\lambda, T)$ of the radiant emanation from the turbine blade measured by the radiation pyrometer can be directly related to the target temperature to be measured T_b. The calculation of the error can be easily performed.

The above analysis discusses the reflective radiation characteristics in the temperature measurement environment of turbine blades during operation, revealing that there are significant reflective radiation measurement errors in turbine blade radiation thermometry. After obtaining the simulation results of the effective emissivity of the turbine blade, the temperature of the target to be measured can be determined using the radiation received by the high-temperature pyrometer. Assuming that the radiation from the high-temperature environment, $M(\lambda, T_r)$, is fully incident on the surface of the target, the temperature measurement algorithm employs the monochromatic temperature measurement method. $M^{-1}\{\lambda, M(\lambda, T)\}$ represents the inverse operation of the Planck formula (Equation (1)), which is used to calculate the corresponding blackbody temperature T when the wavelength$\lambda$and radiation quantity $M(\lambda, T)$ are known. The calculation process is shown in Equation (14). Thus, the radiation measurement error ΔT, caused by the interference of reflective radiation, can be calculated using Equation (15).

$$T=M^{-1}\{\lambda, M(\lambda, T)\}=\frac{c_2}{\lambda\ln\left[\frac{c_1}{\lambda^5 M(\lambda, T)}+1\right]} \tag{14}$$

$$\Delta T=M^{-1}\left\{\lambda, \frac{\varepsilon_{eff}\cdot M(\lambda, T_b)}{\varepsilon}\right\}-M^{-1}\left\{\lambda, \frac{\varepsilon M(\lambda, T_b)}{\varepsilon}\right\} \tag{15}$$

3 Results and Discussion

3.1 Viewfactor Simulation

The three-dimensional discretized radiation transfer model allows us to obtain the coordinate information of each point on the blade surface and calculate the viewfactors between the surface elements based on these coordinates using the triangular face element method. In this paper, the suction surface of the moving blade to be measured at 60% of the blade height is taken as the object of study, as shown by the red dashed line in Fig. 9(a). The triangular method is used to calculate the values of the viewfactors of the neighboring guide vanes to be measured on the moving vane when the relative chord length is between 0 and 1. The results are shown in Fig. 9 (b). The horizontal coordinates in the figure indicate the relative chord length of the suction surface of the turbine blade, and the magnitude of the values corresponds to the leading edge to the trailing edge of the suction surface from left to right, respectively. Due to the structural characteristics of the moving vane and the relative positional relationship with the guide vanes, the variation values of the viewfactors of the neighboring guide vanes to be measured for the moving vane show a decreasing trend.

Based on the model, a measurement point is selected

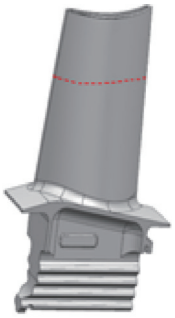

(a) 60% blade height scanning path

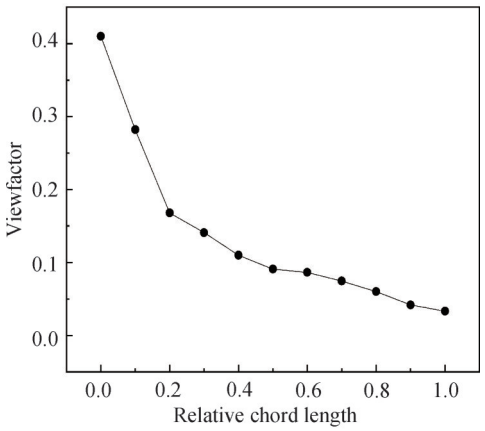

(b) Viewfactor calculation result

Fig.9 (a) 60% blade height scanning path
(b) Viewfactor calculation result

at the suction surface P_0 (with a relative chord length of 0.2 and a relative blade height of 0.6). During one rotation period of the moving blade (i.e., from 0° to 4.2°), the relative position between the front-stage moving blade and the measurement point remains unchanged. Therefore, the influence of the front-stage moving blade on the measurement point is essentially constant. As a result, the focus of this study is on the variation of the viewfactors due to the front-stage guide vanes at the measurement point.

By simulating the motion of the measurement point at different positions within one rotation period, the distribution of the radiation angle coefficients of the guide blades 1, 2, and 3 on the target blade can be observed. Over a full rotation period, moving blade 1 moves along the motion direction to position blade 2, and the variation in the viewfactors of guide vanes 1, 2, and 3 on the measurement point P_0 at different angles is shown in Fig. 10(a)–(c).

From Fig. 10(a), it can be observed that within one rotation cycle of the moving blade, i.e., when the rotation angle ranges from 0° to 4.2°, the viewfactor influenced by guide blade 1 decreases. This is because the effective radiative surface of guide blade 1 on the measurement point gradually diminishes and tends toward zero. On the other hand, the viewfactor influenced by guide blade 2 initially increases and then decreases. During the rotation angle range of 0° to 2°, the measurement point moves

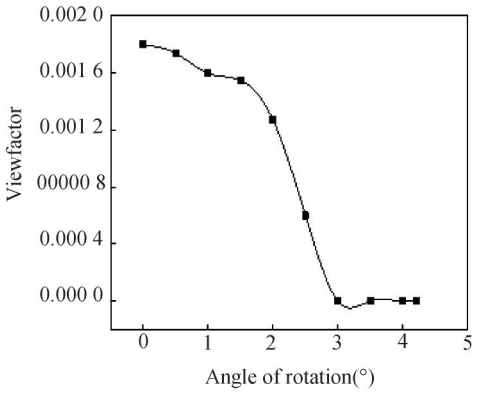

(a) Viewfactor of guide vane 1

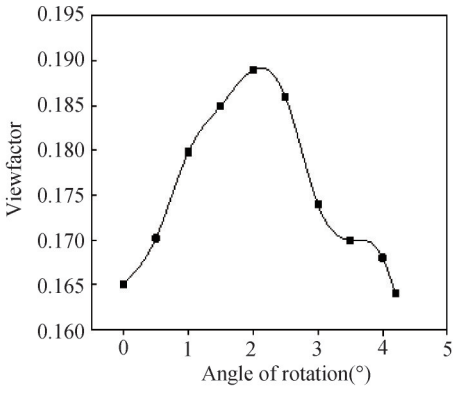

(b) Viewfactor of guide vane 2

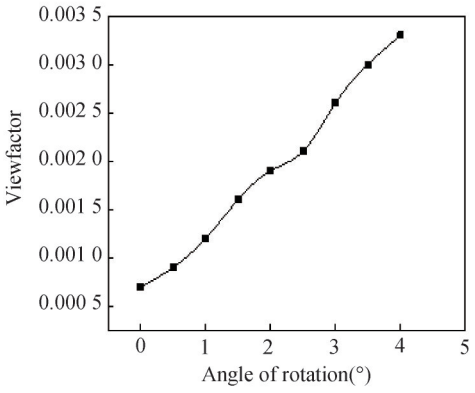

(c) Viewfactor of guide vane 3

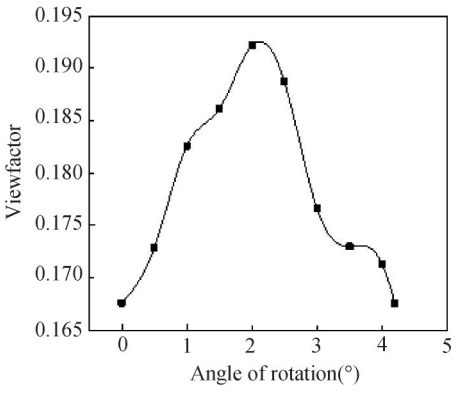

(d) Total viewfactor

Fig.10 The test point is subjected to continuous changes in the viewfactor of the guide vane at different angles
(a) Viewfactor of guide vane 1(b) Viewfactor of guide vane 2(c) Viewfactor of guide vane 3(d) Total viewfactor

closer to guide blade 2, and its effective radiative surface increases, leading to an increase in the viewfactor. However, during the rotation angle range of 2° to 4.2°, the effective radiative surface between guide blade 2 and the measurement point gradually decreases, resulting in a decrease in the viewfactor.

Fig. 10(d) shows the variation in the angle coefficients influenced by all three guide blades on the measurement point over the entire rotation cycle. The overall trend indicates that the angle coefficient first increases and then decreases. Additionally, at the start (0°) and end (4.2°) of the rotation, the viewfactor values are the same, reflecting the periodic variation of the angle coefficient over one full cycle.

To further investigate the radiative influence of nearby guide vanes, a simulation was conducted for the radiation viewfactor at the moment the moving blade rotates to 0°、2°and 4°. In this simulation, 36 measurement points were selected along the moving blade to compute the viewfactor distribution at that specific position. The results of the calculation are shown in Fig. 11.

From Fig. 11, it can be seen that at the different rotation angle, the radiation angle coefficient in the relative chord length range of 0 to 0.2 is generally higher. This is primarily due to the fact that this region is closer to the front-stage guide vanes, and the radiative transfer path is not obstructed by the adjacent moving blade. As a result, the viewfactor reaches its peak in this region, with a significant impact from the reflected radiation. In contrast, in the relative chord length range of 0.2 to 1, the radiation viewfactor is lower, as the influence of reflected radiation decreases. Particularly at a relative chord length of 1, the viewfactor is the lowest, mainly due to the shadowing effect of the blade itself, which minimizes the reflected radiation in this region. During the rotation of the target blade, the position most strongly influenced by the radiation from the three guide vanes is always the leading edge of the suction surface. This position is closest to the guide vanes, resulting in the highest radiative influence. In contrast, the radiation viewfactor at the trailing edge of the suction surface is nearly zero because this position is the farthest from the guide vanes, and thus experiences the least radiative influence. The variation trend of reflected radiation is similar to that of the radiation viewfactor, and thus, it will not be discussed further here.

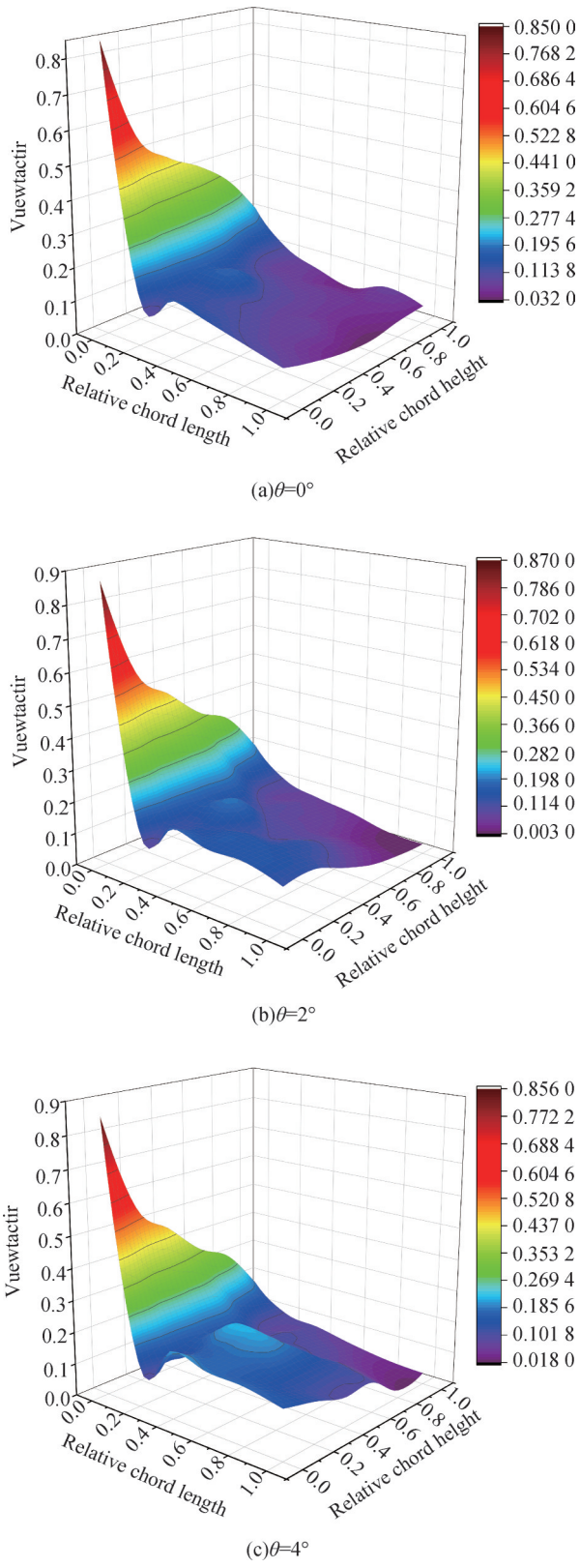

Fig.11 Distribution of radiation viewfactor of adjacent guide vanes on the moving blade at different rotation angle

3.2 Effective Emissivity Calculation

Due to the influence of high-temperature background reflected radiation, there is a significant difference between the effective emissivity and the true emissivity of the turbine blade. The main factors affecting the effective emissivity include the emissivity of the measurement surface of the blade, the measurement wavelength, and the radiation from the high-temperature environment. Fig. 12 show the simulation results of the effective emissivity of the turbine blade when the moving blade rotates to 0°、2° and 4°, with an emissivity of 0.58 and a measurement wavelength of 1.6μm. From the figures, it is clear that at the same rotation angle, the positions with higher reflected radiation correspond to larger effective emissivity values. Notably, at the location where the relative chord length and relative blade height

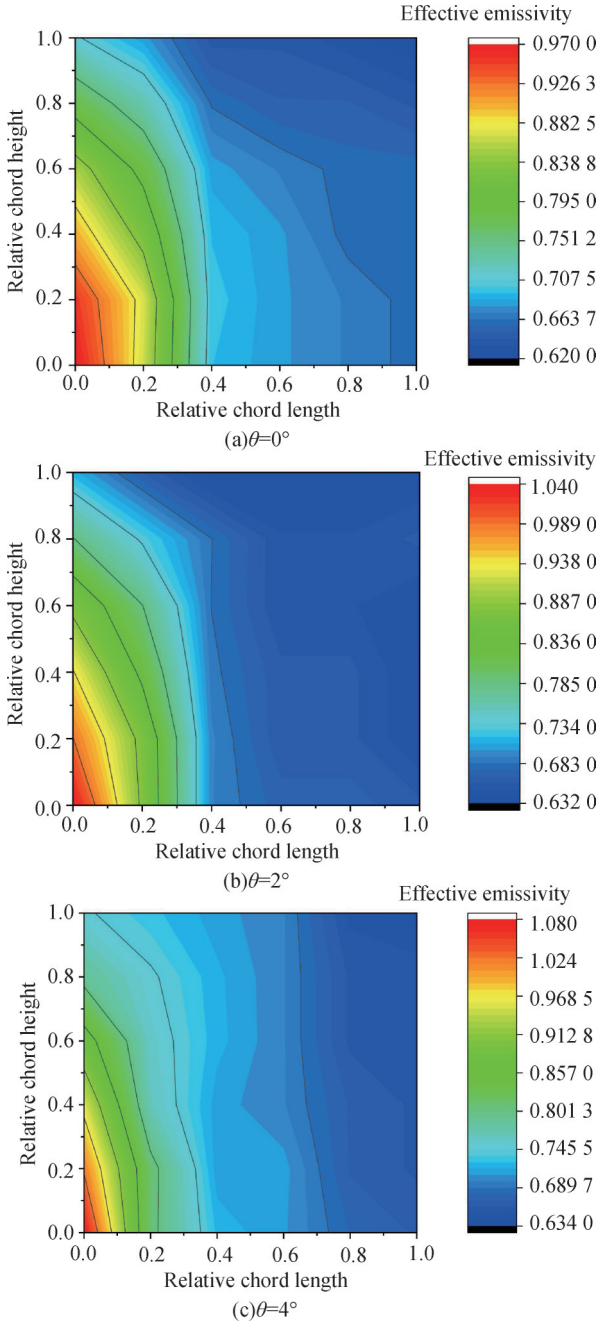

Fig.12 Simulation results of effective emissivity at different rotation angle

are both 0, the effective emissivity reaches its maximum value. Specifically, The maximum values of effective emissivity are 0.97, 1.04 and 1.08 at rotation angles of 0, 2 and 4 deg. It can be seen that the maximum value of effective emissivity increases when the rotation angle increases. It can be seen that the value of effective emissivity is not limited by the value range of 0-1. Effective emissivity can simplify temperature calculations and correct errors, thereby improving real-time measurement and providing data support for further error calculations.

3.3 Error Simulation Analysis

The relative position coordinates of the test point P_0 are selected as (0.2, 0.6). Under the conditions of a measurement wavelength of 1.6μm, emissivity of 0.58, and target blade temperature of 800K, the simulation results of the effective emissivity of the turbine blade at different rotational angles are obtained through Equations (12) and (13). The variation pattern of the radiation temperature measurement error caused by reflected radiation interference when P_0 rotates from 0° to 4° is shown in Fig. 13. With the emissivity, measurement wavelength, and test temperature remaining unchanged, the radiation temperature measurement error caused by reflected radiation fluctuates within the range of 21K to 26K as the rotational angle changes, with a small variation and continuous values. It can be seen that the radiation influence of the pressure side near the moving blade plays a dominant role, and during the rotational process of the test moving blade, the relative position between the moving blades remains unchanged.

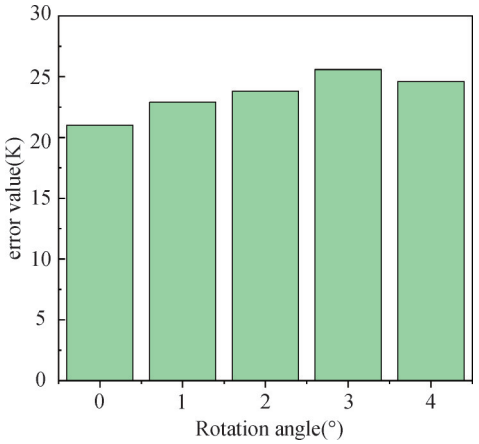

Fig.13 Temperature measurement error distribution with rotation angle

The effect of selecting different points to be measured on the temperature error is considered. The position of the blade height was chosen as 20%, 40%, and 60% to evaluate the effect of reflected radiation on the temperature measurement accuracy at different heights. The temperature error distribution of the blade at different blade heights with rotation Angle is shown in Fig. 14. Under the premise of keeping the emissivity, wavelength and temperature to be measured unchanged, the temperature errors at each leaf height position show a certain fluctuating trend with the change of rotation angle. The largest fluctuation range of temperature error is found at 20% of leaf height, with the maximum error value of 45.14 K. The corresponding range of error at 40% of leaf height is 36.34 K, while at 60% of leaf height, the maximum error decreases to 25.58 K. It can be seen that with the increase of the leaf height, the influence of the rotational angle on the radiometric temperature measurement error tends to be weakened. In addition, the overall error level is significantly higher at 20% leaf height compared to the center and top regions, indicating that this region is more susceptible to

interference from high-temperature background reflected radiation, which leads to larger temperature measurement deviations.

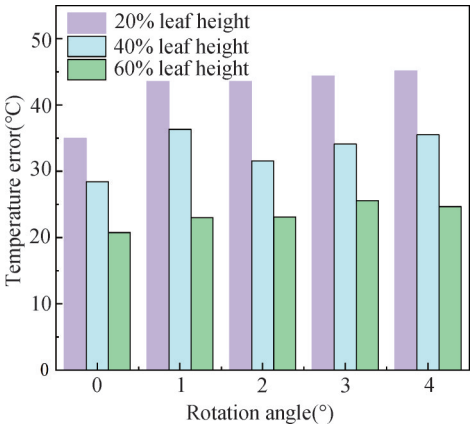

Fig.14 Temperature error distribution with respect to rotation angle at different leaf heights

4 Conclusion

This study provides a feasible error correction method for dynamic temperature monitoring of aero-engine turbine blades, which is especially suitable for non-contact temperature measurement scenarios in high-temperature and strong-reflection backgrounds, and can improve the safety of engine operation and the accuracy of life prediction. The following conclusions are obtained through simulation verification:

(1) This paper accurately describes the reflected radiation transmission relationship between the moving blades and guide vanes under high temperature background by constructing a three-dimensional dynamic radiation transmission model and combining with the periodic motion characteristics of the turbine blades. The model is able to quantify the dynamic change of reflected radiation during the rotation process, which provides a theoretical basis for temperature error correction.

(2) The triangular surface element method is adopted to calculate the radiation angular coefficient, and the effective surface elements are screened by combining the visibility and occlusion relationship, which improves the calculation efficiency. The simulation results show that the angular coefficient shows periodic fluctuation with the change of rotation angle, and the influence is largest in the leading edge region of the dynamic lobe (relative chord length 0-0.2) and smaller in the trailing edge region (relative chord length 0.2-1).

(3) A temperature error calculation method based on the effective emissivity is proposed, which comprehensively considers the effects of the actual emissivity, angular coefficient and background temperature, and simplifies the traditional complex correction process. The simulation results show that the effective emissivity changes dynamically during the rotation process, and the maximum value of the effective emissivity increases with the increase of the rotation angle.

(4) Further analyze the temperature error distribution law at different leaf height positions. With the increase of the leaf height, the influence of reflected radiation on radiation temperature measurement error is weakened. In addition, the overall error level at 20% leaf height is significantly higher compared to the middle and top regions, indicating that this region is more susceptible to the interference of high-temperature background reflected radiation, which leads to larger temperature measurement deviations.

However, the current study does not consider the coupling effect of the dynamic change of the non-uniform temperature field on the reflected radiation in the actual working conditions. Moreover, the current cycle analysis is based on a 4.2° rotation range, which is not extended to the full operating conditions. This limitation needs to be improved subsequently.

Author Contribution:

Shengnan Liu: Conducted raw data collection and performed preliminary analysis; Designed and executed experimental procedures; Created visualizations including graphs and diagrams; Drafted the initial manuscript sections (Introduction, Methods, Results); Participated in critical discussions to refine interpretations. Liwei Chen: Conceptualized the study framework and validated the study design, supervised the study execution; critically revised the intellectual content of the manuscript (including discussion and conclusions); approved the final version for submission.

Funding Information:

This research received no external funding.

Data Availability:

The authors declare that the main data supporting the findings of this study are available within the paper and its Supplementary Information files.

Conflicts of Interest:

The authors declare no competing interests.

Dates:

Received 18 March 2025; Accepted 26 May 2025; Published online 30 June 2025

References

[1] F. Kocian, P. B. Ebel, B. Drees, K. Schulze, J. Hausmann, and H. Voggenreiter, "Hybrid structures in aero engines," *CEAS Aeronautical Journal* , vol. 6, no. 2, pp. 217-228, **2015**.

[2] A. Behera, A. K. Sahoo, and S. S. Mahapatra, "Application of Ni-based superalloy in aero turbine blade: A review," **2023**.

[3] N. Hu, W. Zhao, X. Jin, and X. Fan, "Advances in application of contact temperature measurement technology for aeroengine blade, " *Advances in Aeronautical Science and*

Engineering , vol. 14, no. 1, pp. 1-12, **2022**.

[4] M. R. Reyhani, M. Alizadeh, A. Fathi, and H. Khaledi, "Turbine Blade Temperature Calculation and Life Estimation-a Sensitivity Analysis," *Propulsion & Power Research* , vol. 2, no. 2, pp. 148-161, **2013**.

[5] J. Choi, S. Wee, J.-M. Koo, E.-S. Chung, S.-H. Kwon, and C.-S. Seok, "Thermo-mechanical fatigue characteristics of CMSX-4 applied to the high-pressure turbine first-stage single-crystal rotor blade, " *Journal of Mechanical Science and Technology* , vol. 34, no. 5, pp. 1855-1862, **2020**.

[6] Y. Liu, G. Xu, Y. Fu, J. Wen, and H. Huang, "Thermal dynamic and failure research on an air-fuel heat exchanger for aero-engine cooling," *Case Studies in Thermal Engineering* , vol. 42, **2023**.

[7] P. Liao, Y. Zhang, G. Zhou, X. Zhang, W. Jiang, and S. Tu, "Creep life assessment of aero-engine recuperator based on continuum damage mechanics approach, " *Frontiers of mechanical engineering* , **2022**.

[8] S. Gao, X. Zhang, L. Chen, Y. Cui, J. Jiang, Z. Zhang, P. Yu, and C. Wang, "Review: radiation temperature measurement methods for engine turbine blades and environment influence, " *Infrared Physics &amp* ; Technology, **2022**.

[9] X. Huang, and W. Miglietti, "Wide gap braze repair of gas turbine blades and vanes-a review," *Journal of Engineering for Gas Turbines and Power* , vol. 134, no. 1, **2012**.

[10] X. Guo, W. Zheng, C. Xiao, L. Li, S. Antonov, Y. Zheng, and Q. Feng, "Evaluation of microstructural degradation in a failed gas turbine blade due to overheating, " *Engineering Failure Analysis* , vol. 103, pp. 308-318, **2019**.

[11] M. Pakmehr, A. Behbahani, N. Houtz, and O. Macmann, "Overview of Modern Instrumentation Technology Concerning Prognostics and Health Management and Control in Aero Turbine Engines."

[12] C. Wang, A. Qiu, Z. Zhang, P. Yu, J. Jia, Y. Niu, S. Gao, and J. Jiang, "Panoramic Scanning Optical Pyrometer for the Temperature Field Measurement of Turbine Components, " *IEEE Transactions on Instrumentation and Measurement* , vol. 71, **2022**.

[13] X. Li, H. Yan, S. Zhao, K. Cheng, J. Chen, and X. Huai, "Influence Factors on the Radiation Temperature Measurement Accuracy of Turbine Blades, " *Journal of Thermal Science* , vol. 34, no. 2, pp. 510-523, **2025**.

[14] S. Gao, C. Feng, L. Wang, and D. Li, "Multi-spectral temperature measurement method for gas turbine blade, " *Optical Review* , vol. 23, no. 1, pp. 17-25, **2016**.

[15] D. H. Shin, M. Kim, J. S. Kim, B. J. Lee, and J. Lee, "Precise infrared thermometry with considering background radiation for gas turbine air cooling application," *International Journal of Thermal Sciences* , vol. 158, **2020**.

[16] J. Hartmann, "*High-temperature measurement techniques for the application in photometry* , radiometry and thermometry," Physics Reports, vol. 469, no. 5-6, pp. 205-269, **2009**.

[17] S. Gao, L. Wang, C. Feng, and K. D. Kipngetich, "Analyzing the influence of combustion gas on a gas turbine by radiation thermometry," Infrared Physics and Technology, vol. 73, pp. 184-193, **2015**.

[18] M. De Lucia, R. De Sabato, P. Nava, and S. Cioncolini, "Temperature measurements in a heavy duty gas turbine using radiation thermometry technique: Error evaluation," *Journal of Engineering for Gas Turbines and Power* , vol. 123, no. 2, pp. 333-339, **2001**.

[19] J. Tian, T. Fu, Q. Xu, and H. Jiang, "Effective Spectral Emissivity of Gas Turbine Blades for Optical Pyrometry, " *Journal of Heat Transfer* , vol. 139, no. 7, **2017**.

[20] S. Gao, L. Wang, C. Feng, Y. Xiao, and K. Daniel, "Monitoring temperature for gas turbine blade: correction of reflection model," *Optical Engineering* , vol. 54, no. 6, pp. 065102, **2015**.

[21] K. D. Kipngetich, C. Feng, and S. Gao, "Reflection error correction of gas turbine blade temperature," Infrared Physics and Technology, vol. 75, pp. 153-159, **2016**.

[22] K. Zheng, J. Lü, Y. Zhao, J. Tao, Y. Qin, Y. Chen, W. Wang, Q. Sun, C. Wang, and J. Liang, "Turbine blade three-wavelength radiation temperature measurement method based on reflection error correction," *Applied Sciences* , vol. 11, no. 9, pp. 3913, **2021**.

[23] Zhang Xianqi. Research on infrared radiation temperature measurement method of turbine blade based on effective emissivity[D]. Harbin Engineering University, **2023**.